Journal of Thermal Analysis and Calorimetry (2019) 138:433–441
https://doi.org/10.1007/s10973-019-08213-9

Experimental and theoretical studies on the thermal decomposition of metformin

Ismail Badran[1] · Azfar Hassan[2] · Abdallah D. Manasrah[2] · Nashaat N. Nassar[2]

Received: 19 September 2018 / Accepted: 22 March 2019 / Published online: 2 April 2019

Abstract

This work is a first attempt to understand the mechanism of metformin thermal decomposition under inert conditions. Thermal gravimetric analysis coupled with mass spectrometry was used to probe the thermal degradation reactions. Density functional theory and second-order perturbation (MP2) theoretical calculations were used to construct a reaction mechanism for metformin decomposition. It was evident that the reactions are initiated via formation of methyl radicals, and ammonia via 1.3-H shift, followed by a series of different secondary reaction pathways. The formation of cyanamide, dimethylamine and HCN were among the main secondary products. The proposed mechanism is important for future treatment of wastewater containing metformin and similar drugs formulations, and their possible conversion to useful commodities.

Keywords Metformin · Thermal analysis · Evolved gas analysis · Mass spectrometry · Decomposition · Reaction mechanism · DFT · MP2

Introduction

Pharmaceuticals and personal care products (PPCPs) are a diverse group of chemical compounds designed to control, prevent and cure diseases and improve human and animal health. The continuous growth in the world population, rapid industrialization and the subsequent increasing investment needed for health-care worldwide have resulted in increased consumption of PPCPs in the past few decades [1]. These PPCPs are relatively stable and cannot be fully assimilated by humans and animals during usage. Thus, they are only partially metabolized and some part is excreted in the urine and feces and can enter wastewater treatment plants or the water environment [2]. Therefore, there is an alarming growth in wastewater pollution due to the progressive increase in PPCPs production. In fact, a number of PPCPs have been widely detected in the effluents of wastewater treatment plants (WTPs), in groundwater, in surface water and even in some drinking water sources [3, 4]. This poses a serious threat to public health and aquatic ecosystems. Moreover, in the current context, the present WTPs cannot completely eliminate the PPCPs [5, 6], and thus, water treatment by this type of waste is challenging and requires serious attention and new approaches to stop pharmaceutical leakage form WTPs. In fact, there are an increasing number of studies showing that PPCPs are directly leaking from WTPs into water resources and affecting both aquatic and human lives [6–10]. Contamination of water resources by a wide list of PPCPs was evident in heavily populated regions in Europe [5, 6, 11, 12], the USA [5, 13, 14], India and China [3, 15].

Among this list of PPCPs is the drug metformin (*N*,*N*-dimethylbiguanide) that was discovered in 1922, and it became the drug of choice to treat type 2 diabetes in the 1950s [6, 14, 16, 17]. Despite its ultimate popularity as an antidiabetic drug, metformin cannot be metabolized by the human body and it is estimated that 70% of this drug is excreted in the urine and feces [12, 18]. For this reason, considerable amounts (up to 100 ppm) of the drug were detected in WTPs effluents [14, 16, 18]. In a recent study

✉ Nashaat N. Nassar
nassar@ucalgary.ca

[1] Present Address: Department of Chemistry, An-Najah National University, P. O. Box 7, Nablus, Palestine

[2] Department of Chemical and Petroleum Engineering, University of Calgary, 2500 University Drive NW, Calgary, AB T2N 1N4, Canada

by Bradley et al. [14], metformin was among a list of pharmaceuticals that are prevalent in water streams in the eastern USA. The authors called for a "critical need" for new approaches to stop pharmaceutical leakage form WTPs. In another study by Kot-Wasik et al. [11], metformin was detected in both treated water and untreated water in WTPs in Poland. Despite the low detected concentrations of the drug, the fact that many living beings are allergic to the drug is very concerning. In addition, the presence of metformin in water sources was shown to have serious impacts on human health [12]. The impact is not limited only to humans but to aquatic life too. Niemuth et al. [19] showed that fish exposure to drug can raise serious concerns on its long-term effects.

For this, we have recently geared our efforts toward exploring new approaches to manage metformin and other medical formulations in WTPs. Many approaches are presently used to purify wastewater from several contaminants. Among them are coagulation and flocculation, filtration, adsorption and advanced oxidation processes (AOPs), such as photocatalytic degradation. Recently, our research group has developed a new generation of nanoadsorbent catalysts, so-called nanosorbcats [20, 21], for the treatment of non-biodegradable organic matters present in industrial effluents, whereby the removal of these wastes takes place by adsorption onto the nanosorbcats, followed by either its catalytic oxidation or thermal decomposition into new commodity chemicals or fuels. This approach is effective in protecting the environment as well as converting waste into value-added products [22]. Currently, we are focusing our efforts on widening the applications of nanosorbcats to clean wastewater containing PPCPs compounds such as metformin.

The catalytic conversion of PPCPs into useful products by either partial oxidation, thermal cracking, or steam gasification requires a deep understanding of the reactions associated with this transformation. Because metformin belongs to the amidine group which contain an amino (–NH_2 and –$N(CH_3)_2$) and imino (–NH) functional groups, they can be promising candidates to form ammonia and valuable amines and amides products [23–25]. To the best of our knowledge, a study of the thermal degradation of metformin is not available yet. This motivated us to study the decomposition chemistry of this type of drugs.

This work presents our investigation on the thermal decomposition of metformin using thermogravimetric analysis coupled with a mass spectrometer. The experiments were performed under inert conditions and in the absence of any catalyst in order to avoid any possible oxidation and focus solely on the thermal reactions. This approach serves two purposes: First, it allows a deeper understanding of the dominating decomposition reaction pathways of metformin at higher temperatures, and second, it paves the way into future studies on metformin and similar compounds in the presence of a catalyst.

In this study, we also used advanced ab initio quantum theoretical calculations to propose and evaluate different reaction mechanisms for metformin decomposition. The calculations employed density functional theory (DFT) to explore the reaction mechanisms. To obtain better computational results, second-order Møller–Plesset perturbation theory (MP2) was also employed to calculate the single point energies of all reaction species.

Experimental

Materials

N,*N*-dimethylbiguanide (99.9%), commonly known as metformin, was obtained from Sigma-Aldrich, (Ontario, Canada) and used as received. N_2 and air gases of UHP grade were obtained from Praxair (Calgary, Canada).

Thermogravimetric analysis (TGA) and mass spectrometry (MS)

In order to track the reaction during metformin decomposition, TGA/differential scanning calorimetry (DSC) using a SDT Q600 analyzer (TA Instruments, Inc., New Castle, DE) was carried out to identify the mass losses and the heat flow during the thermal decomposition reaction. The thermogravimetric data were then compared to those of an evolved gas analysis (EGA) that used an online mass spectrometer (Pfeiffer Vacuum GSD 301 O_2, Omnistar, Germany) connected to the TGA/DSC system using a 10-cm-long and 3.175-cm-inner-diameter stainless steel tubing. The produced gases were detected to determine the reaction mechanisms that were taking place during the metformin decomposition. The inlet to the mass spectrometer from the TGA system was kept heated at around 250 °C using heating tapes to avoid condensation of the volatiles and gases produced during the reaction. About 30 mg of the sample was heated under inert conditions (N_2 flow = 50 cm^3 min^{-1}) at a heating rate of 2 °C min^{-1} up to 800 °C. Evolved gas analysis (EGA) was performed by connecting the MS to the outlet of the thermal analyzer.

Theoretical calculations

The theoretical calculations employed in this work were described in details in our previous studies [26–28]. All reactants, intermediates, transition states and products were optimized to their equilibrium geometries using Gaussian 16 [29] and viewed using Gaussview [30]. The optimization was performed using the density functional theory

(DFT) functional B3LYP [31] along with the 6-31+G(d,p) basis set, which proved to be a good method to optimize similar systems [26–28, 32]. In each optimization, a frequency calculation was requested after successful optimization at the same level of theory in order to characterize the structures' minima. Therefore, no imaginary frequencies were observed. Transition states, however, were identified by observing their one and only one imaginary frequency along the desired reaction coordinate. Also, intrinsic reaction coordinates (IRC) was calculated for each TS to validate its authenticity. Zero-point energies (ZPE) were scaled by a factor of 0.9806 as suggested by Scott and Radom [33]. The *singlet* ground state was assumed for all closed shell species unless mentioned otherwise. For open-shell free radicals and intermediates, the unrestricted version of the functional, i.e., uB3LYP, was used.

In order to obtain better final energies, the second-order Møller–Plesset perturbation theory (MP2) [34, 35] was implemented with the 6-311+G(d,p) basis set to calculate the single point energies of all species. Further details on the calculations of the thermochemical parameters: enthalpy, entropy and Gibbs free energy involved in this work, can be found in the previous work [26, 27].

Results and discussion

Experimental data collected by the TGA/MS helped to clarify the reaction mechanism during the thermal decomposition of metformin. Figure 1 displays the TGA data where mass loss and heat flow are plotted against temperature. The figure is also supported by Fig. 2, which displays the gas analysis performed by MS during the TGA run. As seen, in the absence of any catalyst and under nitrogen atmosphere, the TGA profile of metformin displays its melting around 220 °C (an endothermic peak with almost no significant mass loss). This observation agrees well with the reported melting point of metformin (222 °C) [36]. As the temperature increases, metformin undergoes a multistep decomposition reaction. The heat profile shows mainly endothermic peaks that correspond to the energy needed for metformin thermal decomposition, without any oxidation under inert conditions. The mass loss that occurred at different stages because of the thermal decomposition is illustrated in Table 1. Between 225 and 250 °C, there is about 13.1% loss of the mass. This loss can be related to the initial cleavage of $–CH_3$ or $–NH_2$ fragment from the parent molecule.

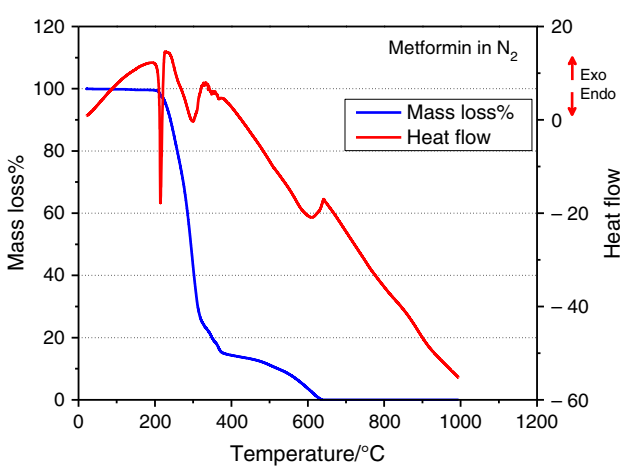

Fig. 1 TG–DTA curve for metformin thermal decomposition at nitrogen flow of 50 cm^3 min^{-1} and heating rate of 2 °C min^{-1}

In Fig. 2, an intense peak for CH_3 (*m/e* 15 molecular ion) in the MS spectrum was observed to increase around 230 °C. However, the intensity of mass peak of NH_2 (*m/e* 16 molecular ion) remained unchanged. This suggests the formation of methyl radicals during the TGA experiments starting at 225 °C.

It is well known that amidines, the class of chemicals that metformin belongs to, form ammonia upon heating [25, 37, 38]. Ammonia is the promising commodity product expected from the catalytic treatment of nitrogen-containing pharmaceutical wastes. As proposed in Scheme 1, ammonia can be directly formed by a 1,3-H shift from NH to the NH_2 terminal in metformin. Using the theoretical methods described in "Theoretical calculations" section, we were able to locate the transition state (TS1) for this shift. An optimized structure for TS1 along with the structure of intermediate **1** is shown in Fig. 3.

As previously noted, the TG–DTA analysis of metformin started with a loss of about 13.1% by mass at 225 °C. This loss can be attributed to ammonia because NH_3 represents 13.2% of metformin by mass. This is supported by the increase in the mass peak at (*m/e* 17 molecular ion) during the TGA/MS analysis described earlier. Also, the relatively low value of E_a (257.4 kJ mol^{-1}) for the formation of ammonia and the almost zero standard $\Delta G°$ of reaction for this pathway are in favor for this interpretation.

In a similar analogy to mechanism A, a 1,3-H shift reaction from –NH to the terminal $–N(CH_3)_2$ group in metformin leads to the formation of dimethylamine (DMA) and intermediate **2** as depicted in Scheme 2. The high instability of intermediate **2** drives it to decompose to a cyclic intermediate **3** which is also in equilibrium with **4**. The two transition states (TS2 and TS3) for this reaction pathways (mechanism B) were successfully located, where Fig. 4 shows their optimized structures along with the intermediate products of this mechanism. This reaction mechanism is supported by the increase in the mass peaks at *m/e* 44 and 45 molecular ions (DMA), and *m/e* 84 and 85 molecular ions resembling intermediate **1**, as seen in Fig. 2.

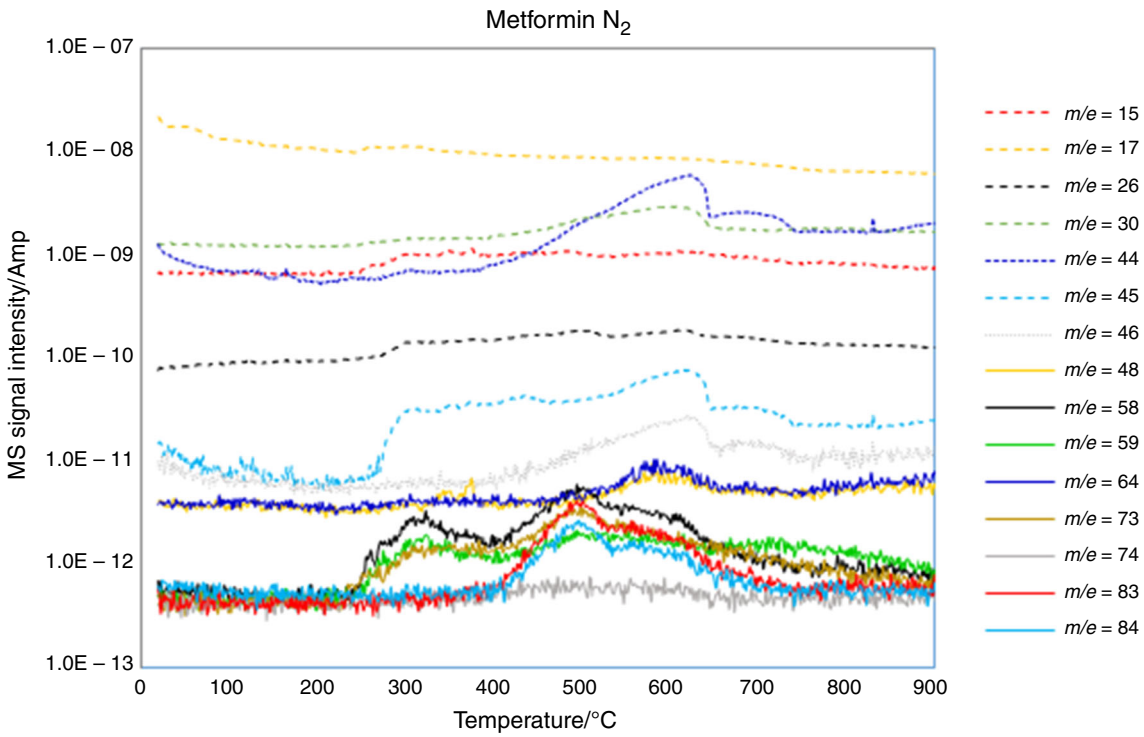

Fig. 2 Mass spectrometric profiles of major products obtained during metformin decomposition under nitrogen atmosphere

Table 1 TG–DTA analysis of metformin pyrolysis at different temperatures

Step	Temperature/°C	Mass loss/%	Heat flow profile	Process
1	220–225	1.8	Sharp endotherm	Melting and loss of adsorbed moisture
2	225–250	13.1	Endotherm	Decomposition
3	250–300	40.4	Broad endotherm	Decomposition
4	300–400	34.2	Small endotherm	Decomposition
5	400–700	14.8	Broad endotherm	Decomposition

Scheme 1 Metformin reaction mechanism A: formation of ammonia

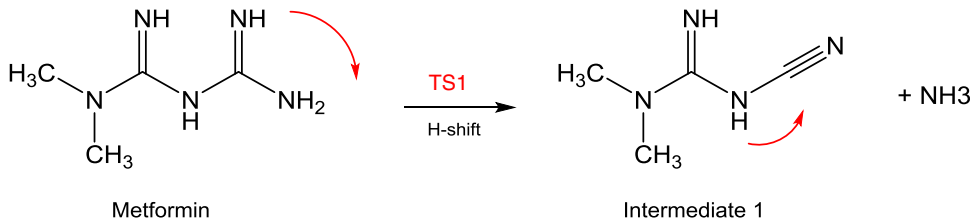

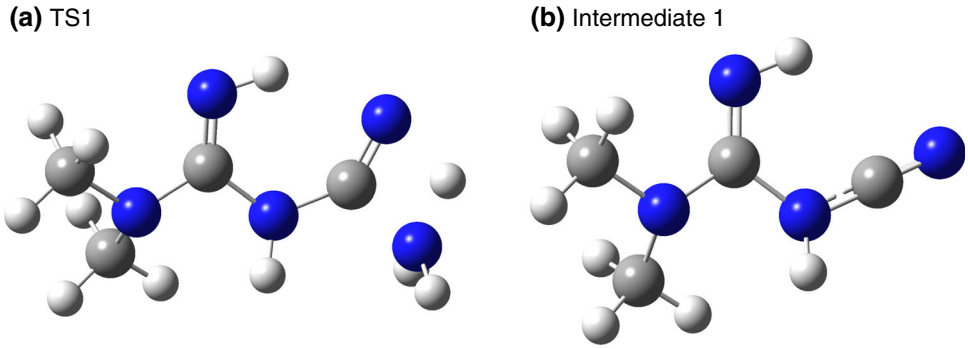

Fig. 3 Optimized structures for **a** the transition state for the 1,3-H shift in metformin leading to the formation of ammonia, and **b** the product of this shift. Both obtained at B3LYP/6-31+G(d,p) level of theory. C atom, gray; N atom, blue. (Color figure online)

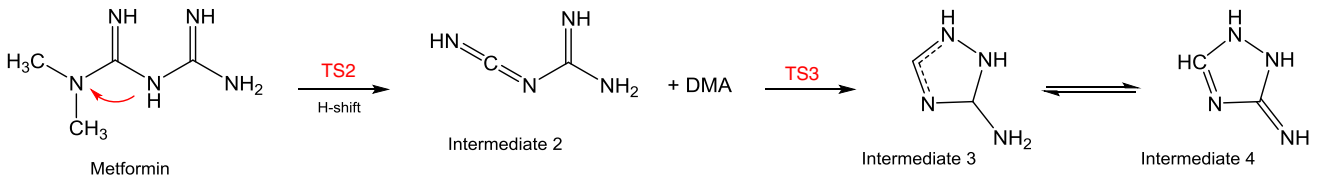

Scheme 2 Metformin reaction mechanism B: formation of dimethylamine

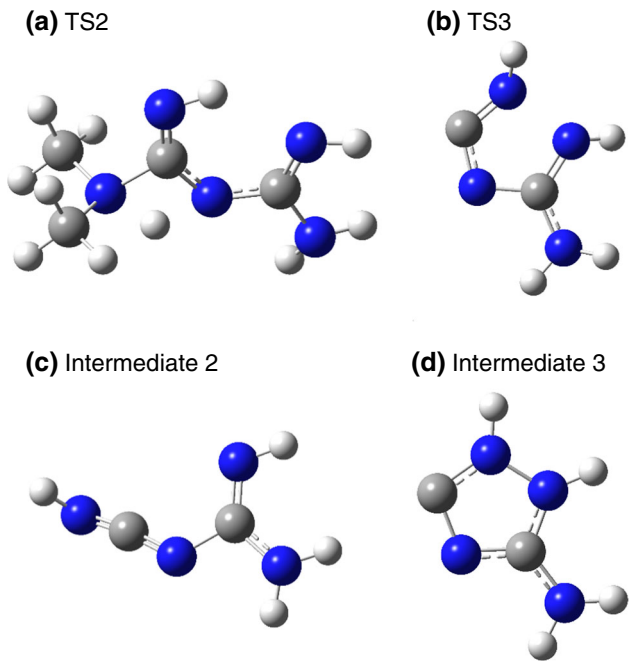

Fig. 4 Optimized structures for the transition states and the intermediate products involved in mechanism B imitated by 1,3-H shift. All obtained at B3LYP/6-31+G(d,p) level of theory. C atom, gray; N atom, blue. (Color figure online)

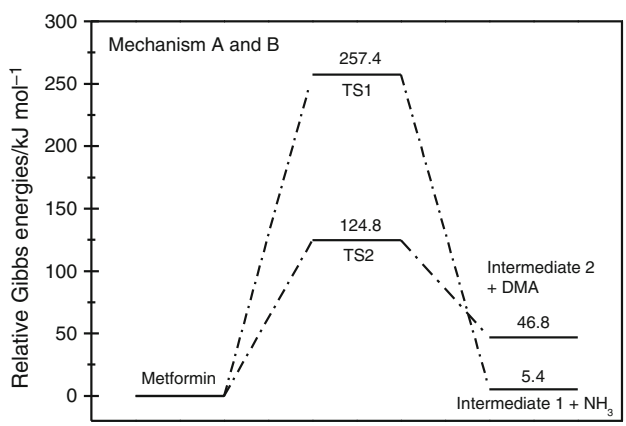

Fig. 5 Potential energy level diagram for reaction mechanisms A and B, formation of ammonia and dimethylamine from metformin initiated by 1,3-H shift. Energies represent relative Gibbs free energies in kJ mol^{-1} at 298 K and 1 atm (ZPE corrections are included)

At the level of theory used in this work, the values of activation barriers (E_a) for the formation of ammonia and DMA are estimated at 257.4 and 124.8 kJ mol^{-1}, respectively (calculated in terms of Gibbs free energies). These values are illustrated in the potential energy diagram in Fig. 5. The Gibbs free energies of reaction ($\Delta G°$) for the formation of ammonia were calculated to be endergonic by 5.4 kJ mol^{-1}, while it was 46.8 kJ mol^{-1} for that of the DMA formation. So, kinetically, DMA formation is preferred over that of ammonia, but the formation of the latter is more thermodynamically favorable.

The fact that the decomposition of metformin started with a mass loss of 13.1%, which could not be originated by DMA, suggests that ammonia formation is experimentally favored over DMA at low temperature. This observation is in concert with the above conclusion that ammonia formation is favored thermodynamically.

This mass loss of 13.1% might also be caused by a loss of –CH_3 or –NH_2 groups as mentioned before. For that, we explored the homolytic bond cleavages in metformin as shown in Scheme 3. In this reaction mechanism, donated C, the major possible bond breaking was explored to produce various free radicals numbered from **5** to **12**.

Conventionally, homolytic cleavages proceed with no barriers, i.e., no transition states [26, 27, 39]. Therefore, we were not able to locate any transition state for the reactions in Scheme 3 except the reaction that is initiated by the rupture of the middle C–N bond in metformin to yield the free radicals **8** and **9**. This transition state, donated TS4, contains an imaginary frequency of 404*i* cm^{-1} that corresponds to the C–N bond stretching.

The potential energy diagram for the reactions of mechanism C is shown in Fig. 6. The standard $\Delta G°$ of reactions for this mechanism ranges between ca. 300 and 410 kJ mol^{-1}, which is typical for the C–N bond dissociation energy [40]. Interestingly, the lowest value of $\Delta G°$ (313.8 kJ mol^{-1}) was found for the methyl group rupture, which also leads to the formation of radical **12**. We mentioned earlier that the first mass loss during to the TG–DTA experiments performed on metformin might correspond to ammonia formation, –CH_3, or –NH_2 ruptures. According to the mass analysis data obtained from the TGA/MS (Fig. 2), only the mass peaks at *m/e* 15 and 17 molecular ions were observed to increase during the experiment (the signal intensity for mass peak at *m/e* 16 molecular ion remained

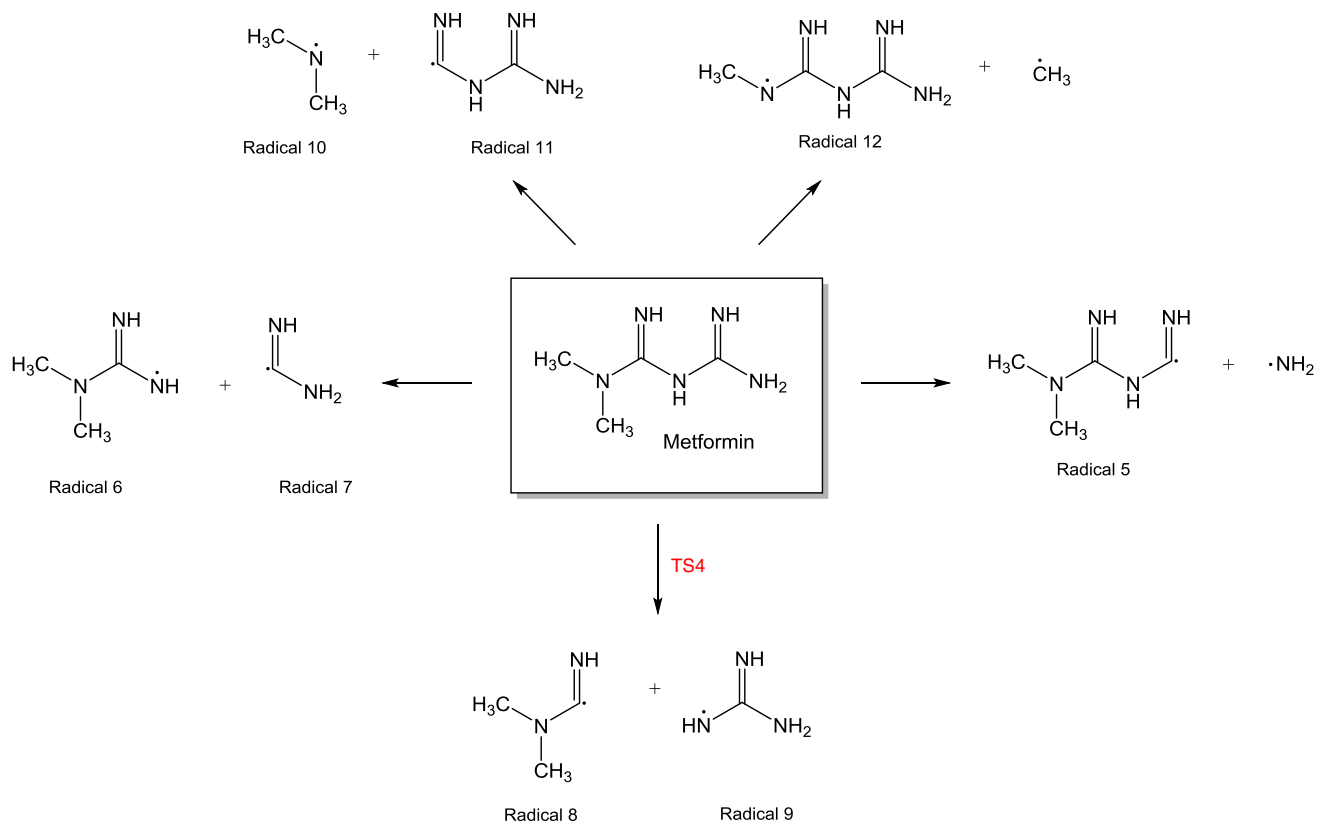

Scheme 3 Reaction mechanism C: homolytic cleavages in metformin

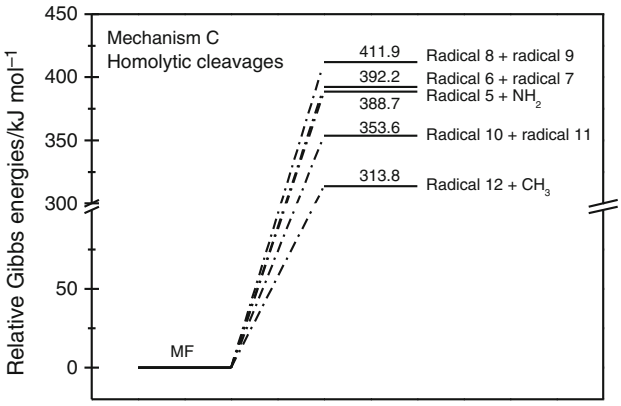

Fig. 6 Potential energy level diagram for reaction mechanism C. Homolytic cleavages in metformin-producing free radicals. Energies represent relative Gibbs free energies in kJ mol^{-1} at 298 K and 1 atm (ZPE corrections are included)

unchanged). The theoretical calculations also suggest a lower barrier for the methyl group formation (313.8 kJ mol^{-1}) compared to that of–NH_2 (388.7 kJ mol^{-1}), as shown in Fig. 6. This explains the absence of any increase in the MS signal intensity for the –NH_2 peak during the TG–DTA experiments. Because ammonia formation is also possible as explained earlier, the mass loss of 13.1% is believed to be related to either ammonia or/and methyl radical formation.

The next mass loss (step 3) during the TG–DTA analysis took place between 250 and 300 °C, and it is about ca. 40% of the remaining solid. This loss can be attributed to the loss of CN_2H_2 fragment from the remaining radical. Theoretically, the CN_2H_2 fragment accounts for 37% of remaining radical, after the initial loss of NH_3, NH_2 or –CH_3. To gain more insights into the nature of this loss (step 3), we explored the secondary decomposition pathways following the first loss. As shown in Scheme 4, there are three possible pathways to form the CN_2H_2 or its radicals. In the first pathway, the intermediate **1**, the product of the initial loss of ammonia, decomposes into radical **13** and cyanamide (CN_2H_2), which accounts for 37.5% of intermediate **1**. In the second pathway, radical **12** formed after an initial methyl radical loss decomposes into radicals **14** and **15** in which radical **15** makes up 37.7% of radical **12**. In the third pathway, radical **5**, which is the product of –NH_2 initial loss, decomposes into radical **16** and the stable cyanamide molecule. In this case, cyanamide accounts for 37.5%. For the first and third pathways in Scheme 4, the transition states, TS5 and TS6, responsible for the reactions could be easily located. The optimized structures for the two TS's are shown in Fig. 7.

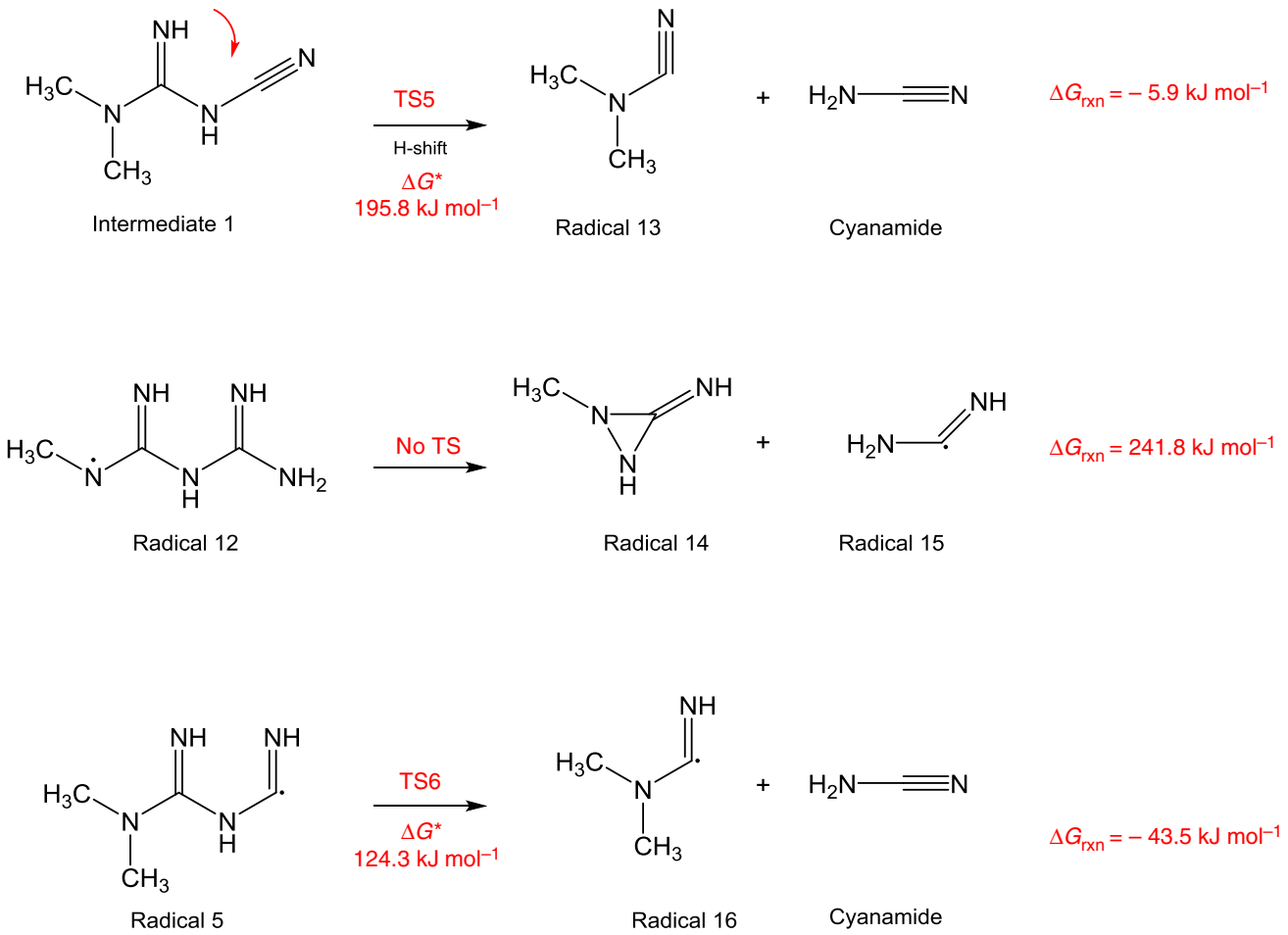

Scheme 4 Secondary decomposition reactions of metformin

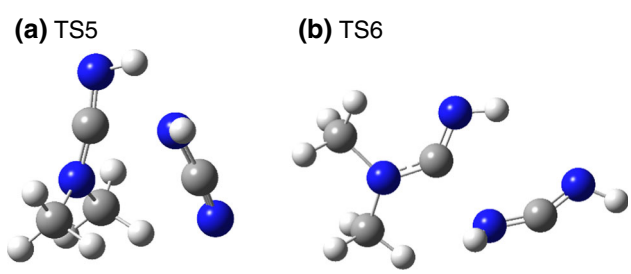

Fig. 7 Optimized structures for the transition states involved in the secondary decomposition reactions of metformin obtained at B3LYP/6-31+G(d,p) level of theory. C atom, gray; N atom, blue. (Color figure online)

Thus, any of the three reactions in Scheme 4 can account for the ca. 40% loss observed in the TG–DTA experiments. Under the level of the theory used in this work, the activation barriers for the first and third reactions in Scheme 4 were calculated to be 159.8 and 124.3 kJ mol^{-1}, respectively, where, as mentioned before, the second reaction proceeds with no transition state, i.e., no barrier. As for the of $\Delta G°$ of reaction, it was calculated to be − 5.9, 241.8 and − 43.5 kJ mol^{-1} for the three reactions, respectively. By observing these values, it is clear that the formation of cyanamide through the third pathway (initial $–NH_2$ loss) is both kinetically and thermodynamically the most favorable one. However, the first step of this reaction pathway, the initial rupture of $–NH_2$, was shown to be both experimentally and theoretically not feasible. By examining the $\Delta G°$ of activations and reactions after ruling out the $–NH_2$ pathway, and based on the fact that formation of the cyanamide-like radical, **15**, through the second pathway (initial $–CH_3$ loss) proceeds with no transition state, it appears that methyl radical pathway is the favored one among those illustrated in Scheme 4. This supports our belief that the 40% mass loss (step 3) from metformin, and consequently its thermal decomposition, is initiated by methyl radical formation and/or ammonia.

In step 4 of the TG–DTA analysis, shown in Fig. 1, a loss of ca. 34.2% by mass was observed between 300 and 400 °C. According to previous studies on amidines [25, 38], HCN was reported to be a major product of their pyrolysis. Interestingly, HCN accounts for 38% of radical

14, which is close to the percentage of mass loss in this step. According to our mass spectrometric analysis, the signal of the peak at *m/e* 27 molecular ion corresponding to HCN remained unchanged during the experiments. This might be due to the low amounts of the gaseous product that could not be detected by the MS.

Conclusions

In this work, the thermal decomposition of metformin was studied experimentally by thermogravimetric analysis and mass spectrometry and theoretically by the density functional theory (DFT) and the second-order perturbation (MP2) theoretical calculations. After its initial melting, the drug went through multistep mass losses that correspond to different decomposition reactions. With the help of quantum theoretical calculations, a full reaction mechanism for metformin decomposition was constructed. By investigating both the experimental and the theoretical results, we concluded that the main thermal decomposition of metformin in the absence of a catalyst is initiated by a methyl radical loss or a 1,3-H shift to form ammonia. This is followed by the formation of cyanamide species and ending up with HCN formation. Other decomposition pathways can have contributions to the decomposition of metformin as well.

The outcomes of this study are significant for the future studies of treating metformin polluted water. More specifically, the potential of producing ammonia and other commodity chemicals from wastewater will be explored using the nanoparticles as adsorbents and catalysts for metformin removal and subsequent catalytic decomposition.

Acknowledgements The authors are grateful to the Natural Sciences and Engineering Research Council of Canada (NSERC) (Grant No. 10010510) and the Department of Chemical and Petroleum Engineering at the Schulich School of Engineering at the University of Calgary for funding this work. This research was enabled in part by support provided by Compute Canada. I. Badran is thankful to the generous support of Zamala, a fellowship provided by Taawon Foundation and Bank of Palestine.

References

1. Van Boeckel TP, Gandra S, Ashok A, Caudron Q, Grenfell BT, Levin SA, et al. Global antibiotic consumption 2000 to 2010: an analysis of national pharmaceutical sales data. Lancet Infect Dis. 2014;14(8):742–50. https://doi.org/10.1016/S1473-3099(14)70780-7.
2. Yan S, Yao B, Lian L, Lu X, Snyder SA, Li R, et al. Development of fluorescence surrogates to predict the photochemical transformation of pharmaceuticals in wastewater effluents. Environ Sci Technol. 2017;51(5):2738–47. https://doi.org/10.1021/acs.est.6b05251.
3. Guan Y, Wang B, Gao Y, Liu W, Zhao X, Huang X, et al. Occurrence and fate of antibiotics in the aqueous environment and their removal by constructed wetlands in China: a review. Pedosphere. 2017;27(1):42–51. https://doi.org/10.1016/S1002-0160(17)60295-9.
4. Masoud MS, Farag HA, Zaatout AA, Kamel HM, ElGreatly MH, Ahmed HM. Recovery of some valuable components from industrial waste. Sep Sci Technol. 2017;52(3):512–9.
5. Luo Y, Guo W, Ngo HH, Nghiem LD, Hai FI, Zhang J, et al. A review on the occurrence of micropollutants in the aquatic environment and their fate and removal during wastewater treatment. Sci Total Environ. 2014;473:619–41.
6. Oosterhuis M, Sacher F, ter Laak TL. Prediction of concentration levels of metformin and other high consumption pharmaceuticals in wastewater and regional surface water based on sales data. Sci Total Environ. 2013;442:380–8.
7. Sarkar S, Das R, Choi H, Bhattacharjee C. Involvement of process parameters and various modes of application of TiO2 nanoparticles in heterogeneous photocatalysis of pharmaceutical wastes—a short review. RSC Adv. 2014;4(100):57250–66. https://doi.org/10.1039/c4ra09582k.
8. De la Cruz N, Esquius L, Grandjean D, Magnet A, Tungler A, de Alencastro LF, et al. Degradation of emergent contaminants by UV, UV/H_2O_2 and neutral photo-Fenton at pilot scale in a domestic wastewater treatment plant. Water Res. 2013;47(15):5836–45. https://doi.org/10.1016/j.watres.2013.07.005.
9. Challis JK, Hanson ML, Friesen KJ, Wong CS. A critical assessment of the photodegradation of pharmaceuticals in aquatic environments: defining our current understanding and identifying knowledge gaps. Environ Sci Process Impacts. 2014;16(4):672–96.
10. Blair B, Nikolaus A, Hedman C, Klaper R, Grundl T. Evaluating the degradation, sorption, and negative mass balances of pharmaceuticals and personal care products during wastewater treatment. Chemosphere. 2015;134:395–401.
11. Kot-Wasik A, Jakimska A, Śliwka-Kaszyńska M. Occurrence and seasonal variations of 25 pharmaceutical residues in wastewater and drinking water treatment plants. Environ Monit Assess. 2016;188(12):661.
12. Kosma CI, Lambropoulou DA, Albanis TA. Comprehensive study of the antidiabetic drug metformin and its transformation product guanylurea in Greek wastewaters. Water Res. 2015;70:436–48. https://doi.org/10.1016/j.watres.2014.12.010.
13. Bollmann AF, Seitz W, Prasse C, Lucke T, Schulz W, Ternes T. Occurrence and fate of amisulpride, sulpiride, and lamotrigine in municipal wastewater treatment plants with biological treatment and ozonation. J Hazard Mater. 2016;320:204–15. https://doi.org/10.1016/j.jhazmat.2016.08.022.
14. Bradley PM, Journey CA, Button DT, Carlisle DM, Clark JM, Mahler BJ, et al. Metformin and other pharmaceuticals widespread in wadeable streams of the southeastern United States. Environ Sci Technol Lett. 2016;3(6):243–9.
15. Yanbo W, Jie F, Sisi Z, Peng S, Yingchun Y. A thermal analysis calculation of pharmaceutical wastewater sludge. J Therm Anal Calorim. 2012;108(1):389–95.
16. Armbruster D, Happel O, Scheurer M, Harms K, Schmidt TC, Brauch H-J. Emerging nitrogenous disinfection byproducts: transformation of the antidiabetic drug metformin during chlorine disinfection of water. Water Res. 2015;79:104–18.
17. Santos A, Basilio I, De Souza F, Medeiros A, Pinto M, De Santana D, et al. Application of thermal analysis in study of binary mixtures with metformin. J Therm Anal Calorim. 2008;93(2):361–4.
18. Quintão FJO, Freitas JRL, de Fátima Machado C, Aquino SF, de Queiroz Silva S, de Cássia Franco Afonso RJ. Characterization of

metformin by-products under photolysis, photocatalysis, ozonation and chlorination by high-performance liquid chromatography coupled to high-resolution mass spectrometry. Rapid Commun Mass Spectrom. 2016;30(21):2360–8.
19. Niemuth NJ, Jordan R, Crago J, Blanksma C, Johnson R, Klaper RD. Metformin exposure at environmentally relevant concentrations causes potential endocrine disruption in adult male fish. Environ Toxicol Chem. 2015;34(2):291–6. https://doi.org/10.1002/etc.2793.
20. El-Qanni A, Nassar NN, Vitale G, Hassan A. Maghemite nanosorbcats for methylene blue adsorption and subsequent catalytic thermo-oxidative decomposition: computational modeling and thermodynamics studies. J Colloid Interface Sci. 2016;461:396–408. https://doi.org/10.1016/j.jcis.2015.09.041.
21. Marei NN, Nassar NN, Hmoudah M, El-Qanni A, Vitale G, Hassan A. Nanosize effects of NiO nanosorbcats on adsorption and catalytic thermo-oxidative decomposition of vacuum residue asphaltenes. Can J Chem Eng. 2017. https://doi.org/10.1002/cjce.22884.
22. Manasrah AD, Nassar NN, Ortega LC. Conversion of petroleum coke into valuable products using oxy-cracking technique. Fuel. 2018;215:865–78.
23. Flinn C, Poirier RA, Sokalski WA. Ab initio study of the deamination of formamidine. J Phys Chem A. 2003;107(50):11174–81.
24. Williams BA, Cool TA. Two-photon spectroscopy of Rydberg states of jet-cooled C_2H_4 and C_2D_4. J Chem Phys. 1991;94(10):6358–66. https://doi.org/10.1063/1.460314.
25. Shriner RL, Neumann FW. The chemistry of the amidines. Chem Rev. 1944;35(3):351–425.
26. Badran I, Rauk A, Shi YJ. Theoretical study on the ring-opening of 1,3-disilacyclobutane and H_2 elimination. J Phys Chem A. 2012;116(48):11806–16. https://doi.org/10.1021/jp3087122.
27. Badran I, Nassar NN, Marei NN, Hassan A. Theoretical and thermogravimetric study on the thermo-oxidative decomposition of Quinolin-65 as an asphaltene model molecule. RSC Adv. 2016;6(59):54418–30. https://doi.org/10.1039/C6RA07761G.
28. Manasrah AD, El-Qanni A, Badran I, Carbognani Ortega L, Perez-Zurita MJ, Nassar NN. Experimental and theoretical studies on oxy-cracking of Quinolin-65 as a model molecule for residual feedstocks. React Chem Eng. 2017;2(5):703–19. https://doi.org/10.1039/C7RE00048K.
29. Frisch M, Trucks G, Schlegel H, Scuseria G, Robb M, Cheeseman J, et al. Gaussian 16, revision A. 03. Wallingford: Gaussian Inc; 2016.
30. Dennington R, Keith T, Millam J. GaussView, version 5. 2009.
31. Becke AD. Density-functional thermochemistry. III. The role of exact exchange. J Chem Phys. 1993;98(7):5648–52.
32. Xiao R, Noerpel M, Ling Luk H, Wei Z, Spinney R. Thermodynamic and kinetic study of ibuprofen with hydroxyl radical: a density functional theory approach. Int J Quantum Chem. 2014;114(1):74–83. https://doi.org/10.1002/qua.24518.
33. Scott AP, Radom L. Harmonic vibrational frequencies: an evaluation of Hartree − Fock, Møller − Plesset, quadratic configuration interaction, density functional theory, and semiempirical scale factors. J Phys Chem. 1996;100(41):16502–13. https://doi.org/10.1021/jp960976r.
34. Head-Gordon M, Pople JA, Frisch MJ. MP2 energy evaluation by direct methods. Chem Phys Lett. 1988;153(6):503–6.
35. Binkley JS, Pople JA. Møller-Plesset theory for atomic ground state energies. Int J Quantum Chem. 1975;9(2):229–36. https://doi.org/10.1002/qua.560090204.
36. Sigma-Aldrich. Metformin, Catalogue number PHR1084 Sigma-Aldrich Corporation. 2018. www.sigmaaldrichchem.com. Accessed 1/7/2018 2018.
37. Andrés J, Beltran A, Carda M, Krechl J, Monterde J, Silla E. Amidine decomposition mechanism. A theoretical study. J Mol Struct (Thoechem). 1992;254:465–72.
38. Andrés J, Krechl J, Silla E. Theoretical study of stationary structures of acetamidine unimolecular decomposition. Chem Phys Lett. 1990;169(6):509–12.
39. Truhlar DG, Garrett BC. Variational transition-state theory. Acc Chem Res. 1980;13(12):440–8. https://doi.org/10.1021/ar50156a002.
40. Smith M, March J. March's advanced organic chemistry: reactions, mechanisms, and structure. 6th ed. Hoboken: Wiley-Interscience; 2007.